

Magneto-optics induced by the spin chirality in itinerant ferromagnet $\text{Nd}_2\text{Mo}_2\text{O}_7$

I. Kézsmárki¹, S. Onoda², Y. Taguchi³, T. Ogasawara⁴, M. Matsubara¹,
S. Iguchi¹, N. Hanasaki¹, N. Nagaosa^{1,4}, and Y. Tokura^{1,2,4}

¹*Department of Applied Physics, University of Tokyo, Tokyo 113-8656, Japan*

²*Spin Superstructure Project, ERATO, Japan Science and Technology Agency,
c/o Department of Applied Physics, University of Tokyo, Tokyo 113-8656, Japan*

³*Institute for Materials Research, Tohoku University, Sendai 980-8577, Japan and*

⁴*Correlated Electron Research Center (CERC), National Institute of
Advanced Industrial Science and Technology (AIST), Tsukuba 305-8562*

(Dated: version November 19, 2018)

It is demonstrated both theoretically and experimentally that the spin chirality associated with a noncoplanar spin configuration produces a magneto-optical effect. Numerical study of the two-band Hubbard model on a triangle cluster shows that the optical Hall conductivity $\sigma_{xy}(\omega)$ is proportional to the spin chirality. The detailed comparative experiments on pyrochlore-type molybdates $R_2\text{Mo}_2\text{O}_7$ with $R = \text{Nd}$ (Ising-like moments) and $R = \text{Gd}$ (Heisenberg-like ones) clearly distinguishes the two mechanisms, i.e., spin chirality and spin-orbit interactions. It is concluded that for $R = \text{Nd}$, $\sigma_{xy}(\omega)$ is dominated by the spin chirality for the dc ($\omega = 0$) and the $d \rightarrow d$ incoherent intraband optical transitions between Mo atoms.

PACS numbers: 78.20.Ls, 78.20.Bh,

Quantum-mechanical phenomena associated with the Berry phase¹ have attracted much interest in condensed-matter physics, including charge and spin Hall transport properties. In particular, it has recently been recognized that the Berry phase is relevant to the anomalous Hall effect (AHE) where a finite dc Hall conductivity $\sigma_{\text{Hall}}(\equiv \sigma_{xy}(\omega = 0))$ appears in ferromagnets. It was first proposed that the AHE originates from a fictitious magnetic flux penetrating the conducting network^{2,3,4}. However, the AHE is distinct from the ordinary Hall effect that appears in the presence of the external uniform magnetic field, since the periodicity of the crystal is preserved in the case of the AHE. Then it was found that the Berry phase curvature of the Bloch wavefunction in the momentum space is a more fundamental and universal concept^{5,6,7,8}, which leads to a finite anomalous contribution to the Hall conductivity. This Berry phase curvature emerges through the relativistic spin-orbit interaction and/or the solid angle subtended by the spins under the noncoplanar structure, the latter of which is called *spin chirality*^{9,10,11,12}.

The spin-chirality mechanism for the AHE has a fundamental significance, since the spin-orbit coupling acting on the propagating carriers was considered to be indispensable to produce the AHE in conventional theories^{13,14}. Recently, spin-chirality scenarios for the AHE have been extensively studied from both theoretical and experimental aspects^{2,3,4,5,6,15,16,17,18}. On the other hand, it is also believed that the spin-orbit coupling is indispensable to have a finite optical Hall conductivity $\sigma_{xy}(\omega)$. It remains as an open issue how such magneto-optical properties are influenced by the spin chirality in strongly correlated electron systems like transition-metal oxides, which is of our interest in the present paper.

In conventional magnets, it is difficult to distinguish between two mechanisms based on the spin-orbit inter-

action and the spin chirality, since the noncoplanar spin structure itself originates mostly from the spin-orbit interaction acting on the same electrons which are responsible for the magnetism. In this context, a pyrochlore molybdate system $R_2\text{Mo}_2\text{O}_7$ ($R = \text{Nd}$ and Gd) offers an ideal laboratory to address this issue⁶.

The both compounds have a unit cell composed of a tetrahedron for R ions and that for Mo which are shifted from each other by half the lattice constant. $\text{Nd}_2\text{Mo}_2\text{O}_7$ henceforth referred to as the NMO is an itinerant ferromagnet with Curie temperature $T_C \sim 90$ K. By a small amount of hole doping, the marginally insulating $\text{Gd}_2\text{Mo}_2\text{O}_7$ turns to be a ferromagnetic metal with $T_c \sim 60$ K in the case of $(\text{Gd}_{0.95}\text{Ca}_{0.05})_2\text{Mo}_2\text{O}_7$ (henceforth referred to as the GMO). The ferromagnetism in these compounds is mostly attributed to the double exchange mechanism for mobile carriers of Mo $4d$ electrons. Well below T_c (~ 40 K for $R = \text{Nd}$), through the exchange coupling J_{fd} with the Mo spins, the localized $4f$ moments on the rare-earth ions $R = \text{Nd}$ and Gd start to produce a net magnetic moment in the anti-parallel and the parallel directions to the ferromagnetic moments of Mo spins, respectively. Here, it is important to notice that the Nd moments are subject to a strong single-ion anisotropy and the four moments in the Nd tetrahedron behave as Ising spins pointing toward or outward the center of the tetrahedron as in spin-ice systems⁶. In contrast, the Gd moments behave as Heisenberg spins since the orbital moment is quenched in the Gd^{3+} ion with the $4f^7$ configuration¹⁶. The noncoplanar spin anisotropy and structure of the Nd moments are transmitted to the Mo spins through the exchange coupling J_{fd} , leading to the spin chirality of the Mo electrons only in the case of the NMO.

This spin chirality manifests itself as a gauge flux which is experienced by the electrons upon their coherent and incoherent propagations, or the optical $d \rightarrow d$ transition

between the Mo atoms, while the local charge transfer excitations on the Mo–O bonds are least influenced by the spin chirality since the oxygen ion has no spin moment. In the dc limit, the spin chirality actually contributes to the AHE. In particular, in the case of the NMO, we can distinguish a *spin chirality induced term* in σ_{Hall} from the conventional one associated with the spin-orbit coupling of the itinerant electrons. This is because the spin chirality of the Mo conduction electrons appears without the spin-orbit interaction acting on themselves. Similarly, it is expected that the *spin chirality* gives an additional contribution to $\sigma_{xy}(\omega)$ for the NMO, as far as the optical $d \rightarrow d$ transitions between the Mo atoms is concerned. Namely, the dc and the optical Hall conductivities of the NMO in the energy range from $\omega = 0$ to the optical $d \rightarrow d$ transitions contain the *spin chirality induced contributions*. On the other hand, those of the GMO, which is a reference system reproducing well the magnetic and longitudinal-transport properties of the NMO except the chiral spin order arise solely from the conventional spin-orbit coupling acting on the Mo $4d$ electrons. Therefore, the comparison between NMO and GMO offers a touchstone for the spin-chirality mechanism. On this basis, we study magneto-optics due to the spin chirality from both the theoretical and the experimental viewpoints.

The Mo^{4+} ion has two $4d$ electrons in the t_{2g} orbital in the local coordinate associated with each MoO_6 octahedron. The trigonal crystal field splits the triply degenerate t_{2g} orbitals into a single a_{1g} and doubly degenerate e_g orbitals. One electron occupied in the a_{1g} orbital is more localized than the other in the e_g orbital^{20,21}. To mimic this situation of NMO and GMO and to gain fundamental magneto-optical properties induced by the spin chirality, we consider the following simplest model Hamiltonian on a triangle cluster;

$$\mathcal{H} = \sum_{i=1}^3 \left[-t \sum_{m,\alpha} (c_{i,m,\alpha}^\dagger c_{i+1,m,\alpha} + \text{h.c.}) - \mathbf{h}_i \cdot \sum_m \mathbf{s}_{i,m} + U \sum_m n_{i,m,\uparrow} n_{i,m,\downarrow} + U' n_{i,1} n_{i,2} - 2J_{\text{H}} \mathbf{s}_{i,1} \cdot \mathbf{s}_{i,2} \right]. \quad (1)$$

Here, $c_{i,m,\alpha}$ and $c_{i,m,\alpha}^\dagger$ are the annihilation and creation operators of electron at the site i with the orbital m ($= 1$ or 2) and the spin α (\uparrow or \downarrow), where the site 4 is identified with 1. (See Figs. 1 (a) and (b).) We have also introduced $n_{i,m,\alpha} \equiv c_{i,m,\alpha}^\dagger c_{i,m,\alpha}$, $n_{i,m} \equiv \sum_\alpha n_{i,m,\alpha}$, and $\mathbf{s}_{i,m} \equiv \frac{1}{2} \sum_{\alpha,\alpha'} c_{i,m,\alpha}^\dagger \boldsymbol{\sigma}_{\alpha\alpha'} c_{i,m,\alpha'}$. t is an orbital-diagonal transfer integral between the nearest neighbors, U and $U' = U - (5/2)J_{\text{H}}$ are the local Coulomb interaction parameters, and J_{H} is the Hund coupling henceforth assumed to be $U/8$. The second term in the square bracket in Eq. (1) mimics the molecular fields created by the a_{1g} and the surrounding e_g electrons as well as the surrounding rare-earth moments in the two-in two-out configuration in the context of the spin ice²². Figure 1 displays the local spin configuration on a Mo tetrahedron which is the magnetic unit cell of the Mo sublattice in pyrochlore-type

molybdates. The collinear case in Fig. 1 (d) corresponds to GMO while the chiral spin order, the so-called “umbrella” structure realized in NMO is shown in Figs. 1 (e) and (f).

With the spin configurations as shown in Figs. 1 (a) and (b), we have numerically calculated the conductivity tensor $\sigma_{\mu\nu}(\omega)$ of this model. When \mathbf{h}_i 's are collinear as in Fig. 1 (a) or even coplanar within the xy plane and hence so is the spin alignment, we obtain $\sigma_{xy}(\omega) = 0$. Now, we introduce the noncoplanar umbrella-like configuration for \mathbf{h}_i as depicted in Fig. 1 (b), where $\mathbf{h}_i = h\mathbf{e}_i$ with $\mathbf{e}_1 = (-\frac{\sqrt{3}}{2}\sin\theta, -\frac{1}{2}\sin\theta, \cos\theta)$, $\mathbf{e}_2 = (\frac{\sqrt{3}}{2}\sin\theta, -\frac{1}{2}\sin\theta, \cos\theta)$ and $\mathbf{e}_3 = (0, \sin\theta, \cos\theta)$ in the range of $0 < \theta < 90^\circ$. In this case, the spin chirality $\chi = \langle \mathbf{S}_1 \times \mathbf{S}_2 \cdot \mathbf{S}_3 \rangle$ emerges, where $\mathbf{S}_i = \mathbf{s}_{i,1} + \mathbf{s}_{i,2}$ is the total spin on the site i .

Figure 1 (g) represents the main structure in the real part $\sigma'_{xy}(\omega)$ of the optical Hall conductivity $\sigma_{xy}(\omega)$ for $0 \leq \theta \leq 10^\circ$. For the collinear case $\theta = 0$ and the coplanar case $\theta = 90^\circ$ (not shown), $\sigma_{xy}(\omega)$ vanishes. With increasing θ from 0, the $\sigma_{xy}(\omega)$ gradually emerges. For the present study of the finite-size cluster which is inherently insulating, the energy scale of $\omega/t \approx 4$ is focused. This spectral region corresponds to incoherent excitations in the case of the bulk system. The θ dependence of the spectral intensity at three different energies are shown in Fig. 1 (h) together with the normalized spin chirality $\tilde{\chi} = \chi / (\langle S_1 \rangle \langle S_2 \rangle \langle S_3 \rangle)$. Here, it is evident that both $\sigma'_{xy}(\omega)$ and $\tilde{\chi}$ are in proportion to θ^2 , and hence $\sigma_{xy}(\omega) \propto \tilde{\chi}$ for such small values of θ . As we increase U , the optical Hall conductivity spectra shift to higher energy with the intensity being decreased. It is notable that a small spin canting affects the magneto-optical response at such incoherent regime. The on-site Coulomb interactions only determine the characteristic excitation energy ω for the incoherent optical process and the longitudinal current response at this energy with the factor $\sim 1/\omega$. The ratio of the anomalous Hall velocity to the longitudinal one is exclusively determined by the tilting angle θ and insensitive to the Coulomb interaction parameters. The triangular-cluster model of non-coplanar spins is the most basic system to investigate the effect of spin chirality on the optical Hall conductivity. Although these results allow at most semi-quantitative comparison with the experiments they generally prove the importance of the spin-chirality contribution to $\sigma_{xy}(\omega)$ in the incoherent range of the spectrum (for intraband transitions or excitations through the gap) independently of the fine details of the model system.

Now we turn to the experimental results. Figure 2 shows the diagonal conductivity spectrum of NMO in the ferromagnetic metallic ground state. As evidenced by a systematic study of the bandwidth controlled metal-insulator transition in pyrochlore molybdates²¹, the $\omega \leq 2$ eV excitations correspond to the Mo $4d$ intraband optical processes. The low-energy side of the conductivity spectrum is well fitted by a Drude term (with a scattering rate of $\gamma \approx 35$ meV) when the contribution of the

infrared active phonon modes is subtracted. The coherence peak is followed by the so-called incoherent band (or intraband) transitions in the mid-infrared region which is characteristic of correlated electron systems in the vicinity of a metal to insulator transition. Separated from the Mo 4d optical processes, the higher energy conductivity peak (centered around ~ 4.4 eV) is assigned as local charge-transfer excitations from oxygen sites to neighboring Mo sites.

The dominance of the spin chirality mechanism over the spin-orbit interaction in the dc AHE of pyrochlore molybdates (namely ~ 2 orders of magnitude difference) has been previously pointed out in frame of a comparative investigation of NMO and GMO⁶. Now, on the basis of the present wide energy-range magneto-optical experiments we shall conclude that the same tendency remains valid for the finite-frequency transverse transport, $\sigma_{xy}(\omega)$, as far as the Mo 4d intraband-transition region is concerned.

Figure 3 gives a comparison between the optical properties of NMO and GMO in their ground state. The measured quantities are shown on the left panel, while real and imaginary parts ($\sigma'_{\mu\nu}(\omega)$ and $\sigma''_{\mu\nu}(\omega)$, respectively) of the conductivity tensor $\sigma_{\mu\nu}(\omega)$ on the right. They are plotted on a common energy scale over the range of the magneto-optical study. $\sigma'_{xx}(\omega)$ was obtained by Kramers-Kronig transformation from the reflectivity, while due to the applied ellipsometric method, $\sigma_{xy}(\omega)$ could be directly determined from the magneto-optical Kerr parameters:

$$\sigma_{xy}(\omega) = -(\Theta_K(\omega) + i\eta_K(\omega))\sigma_{xx}(\omega)\sqrt{1 + 4\pi i\sigma_{xx}(\omega)/\omega}, \quad (2)$$

where $\Theta_K(\omega)$ and $\eta_K(\omega)$ are the Kerr rotation and the Kerr ellipticity, respectively, measured by a polarization modulation technique²³. For both compounds, with nearly normal incidence, the polar Kerr spectra of the (100) crystallographic plane were measured in a magnetic field of $B = 0.26$ T in the temperature range of $T = 10 - 120$ K. This magnetic field is large enough to orientate the ferromagnetic domains but still can be considered as the zero-field limit.

Both compounds can be classified as bad metals since even at the lowest temperature the resistivity is close to or even larger than the Ioffe-Regel limit ($\rho_{I-R} \approx 0.53$ m Ω cm) (see Fig. 3). The whole σ_{xx} spectra are also similar to each other in magnitude. By contrast, we have observed large signals Θ_K and η_K for NMO below ~ 2 eV, while substantially smaller ones for GMO. In both cases, there appear a peak structure in $\Theta_K(\omega)$ and the corresponding inflection in $\eta_K(\omega)$ centered around ~ 1 eV, but these are due to the presence of the apparent plasma edge (indicated by a dashed line). After evaluating $\sigma_{xy}(\omega)$ according to Eq. (2) the apparent plasma resonance is naturally cancelled out by the energy dependence of $\sigma_{xx}(\omega)$, which ensures the correctness of the Kramers-Kronig transformation. Nevertheless, a significant difference is quite clear in the magnitude of $\sigma_{xy}(\omega)$ for the infrared incoherent band ($\omega \lesssim 1$ eV) between the

two compounds.

On the high-energy side which is dominated by the O $2p \rightarrow$ Mo 4d charge-transfer excitations, the magneto-optical response of the two systems are almost identical. This suggests that in this energy region, $\sigma_{xy}(\omega)$ solely originates from the spin-orbit interaction of the Mo electrons and simply measure the spin polarization of the final state (not the chirality), therefore invariant under the change of the rare-earth component. Towards lower energies where the Mo 4d intraband transitions are dominant, however, $\sigma_{xy}(\omega)$ shows a robust increase in the case of NMO while not for GMO. At the lowest energy of the experiment, $\omega = 0.11$ eV, this tendency results in nearly one order of magnitude difference between the magneto-optical responses of the two compounds, as expressed by $\sigma'_{xy}(\text{NMO})/\sigma'_{xy}(\text{GMO}) \approx 6.5$ and $\sigma''_{xy}(\text{NMO})/\sigma''_{xy}(\text{GMO}) \approx 11.4$.

In Fig. 4, we present the detailed temperature dependence of $\sigma_{xy}(\omega)$ for NMO. The spectral structure does not vary with increasing temperature, but only its magnitude is suppressed as T_c is approached. Figure 4 shows the temperature dependence of $\sigma_{xy}(\omega)$ for the both compounds at three representative energies: (i) in the dc limit, (ii) in the region of the incoherent intraband transitions ($\omega = 0.11$ eV) and (iii) for the charge-transfer peak ($\omega = 4.4$ eV). The total magnetization and the Mo-spin contribution⁶ are also plotted in the same figure. Below 50 K, the Nd moments tend to align antiparallel to the almost ferromagnetically ordered Mo spins which results in the low-temperature reduction of the magnetization. By contrast, the interaction between Mo and Gd sites is ferromagnetic, and hence the magnetization is enhanced in GMO. As far as the Mo 4d intraband (incoherent band) transitions at 0.1 – 1 eV are concerned, $\sigma_{xy}(\omega)$ of NMO is substantially larger than that of GMO over the whole ferromagnetic phase of the compounds, independently of temperature. This key finding evidences that the leading term in the magneto-optical response of the incoherently moving electrons comes from the spin-chirality mechanism.

Generally speaking, the role of the spin chirality becomes more important as the dc limit is approached, since the low-energy transitions can more coherently pick up the gauge flux (or integrate the Berry curvature). When the Fermi level is located within a tiny energy gap generated by the gauge flux at the band crossing point, $\sigma_{xy}(\omega=0)$ is maximized due to the presence of the magnetic-monopole analog at the crossing point⁸. In the low-temperature phase of NMO, this characteristic energy scale is estimated to be $E_0 \sim 0.02$ eV²⁵. The temperature dependence of $\sigma_{xy}(\omega)$ should show a complicated behavior for $\omega < E_0$ as a finger print of this gauge flux structure in momentum space. For $\omega \gg E_0$, on the other hand, the perturbative treatment of the magnetization M times the spin chirality χ is appropriate, and hence we predict $\sigma_{xy} \propto \theta^2 M$. Therefore, considering $E_0 < 0.1$ eV, it is reasonable that the temperature dependence of $\sigma_{xy}(\omega)$ in Figs. 4 and 5 scales with the Mo

magnetization except the dc value.

A nonmonotonous spectral shape of $\sigma_{xy}(\omega)$ is expected for $\omega < 0.1$ eV, since it is known that complicated band crossings realized in the electronic structure gives a rapid oscillation of $\sigma_{xy}(\omega)$ as mentioned above. Indeed, it is discerned in the low-energy $\sigma_{xy}(\omega)$ spectra of NMO. Furthermore, $\sigma_{xy}''(\omega)$ obviously changes sign at ~ 0.1 eV. From the Kramers-Kronig relation, this has to be accompanied by a maximum in $\sigma_{xy}'(\omega)$. Similarly, one can show that the compatibility of the dc values ($\sigma_{xy}'(\omega = 0) > 0$ and $\sigma_{xy}''(\omega = 0) = 0$) with the low-energy $\sigma_{xy}(\omega)$ data presented in Fig. 4, $\sigma_{xy}'(\omega)$ requires two more sign changes in the experimentally inaccessible low-energy region as the dc limit is approached. Such a behavior is consistent with the above scenario of the rapid oscillation of $\sigma_{xy}'(\omega)$ at low energies due to the band crossing.

In conclusion, we have demonstrated, theoretically and experimentally, the magneto-optical effect induced by the spin chirality. The theory on the two-band Hubbard model for a triangle cluster shows that the optical Hall conductivity across the Mott-Hubbard gap emerges in the presence of the spin chirality. The magneto-optical experiments have shown that the amplitude of the optical Hall conductivity in the energy range of $d \rightarrow d$ intraband transitions between the Mo atoms is large under a noncoplanar spin structure in $\text{Nd}_2\text{Mo}_2\text{O}_7$ with spin chirality, while it is significantly suppressed in $\text{Gd}_2\text{Mo}_2\text{O}_7$ without spin chirality.

This work was in part supported by a Grant-In-Aid for Scientific Research from the MEXT, Japan. I. K. acknowledges support from JSPS.

- ¹ M. V. Berry, Proc. R. Soc. Lond. **A392**, 45 (1984).
- ² P. Matl *et al.*, Phys. Rev. B **57**, 10248 (1998).
- ³ J. Ye *et al.*, Phys. Rev. Lett. **83**, 3737 (1999).
- ⁴ Y. Lyanda-Geller *et al.*, Phys. Rev. B **63**, 184426 (2001).
- ⁵ K. Ohgushi, S. Murakami, and N. Nagaosa, Phys. Rev. B **62**, R6065 (2000).
- ⁶ Y. Taguchi, Y. Oohara, H. Yoshizawa, N. Nagaosa, and Y. Tokura, Science **291**, 2573 (2001).
- ⁷ M. Onoda and N. Nagaosa, J. Phys. Soc. Jpn. **71**, 19 (2002); T. Jungwirth, Q. Niu, and A. H. MacDonald, Phys. Rev. Lett. **88**, 207208 (2002).
- ⁸ Z. Fang *et al.*, Science **302**, 92 (2003).
- ⁹ G. Baskaran and P. W. Anderson, Phys. Rev. B **37**, R580 (1988).
- ¹⁰ R. B. Laughlin, Science **242**, 525 (1988).
- ¹¹ X. G. Wen, F. Wilczek, and A. Zee, Phys. Rev. B **39**, 11413 (1989).
- ¹² P.A. Lee and N. Nagaosa, Phys. Rev. B **46**, 5621 (1992).
- ¹³ R. Karplus and J. M. Luttinger, Phys. Rev. **95**, 1154 (1954).
- ¹⁴ J. Kondo, Prog. Theor. Phys. **27**, 772 (1962).
- ¹⁵ S. Onoda and N. Nagaosa, Phys. Rev. Lett. **90**, 196602 (2003).
- ¹⁶ Y. Taguchi *et al.*, Phys. Rev. Lett. **90**, 257202 (2003).
- ¹⁷ S. Iguchi, D. Hashimoto, Y. Taguchi, and Y. Tokura, Phys. Rev. B **69**, 220401(R) (2004).
- ¹⁸ G. Tatara and H. Kawamura, J. Phys. Soc. Jpn. **71**, 2613 (2002).
- ¹⁹ T. Moriya, Phys. Rev. **120**, 91 (1960).
- ²⁰ I. V. Solov'yev, Phys. Rev. B **67**, 174406 (2003).
- ²¹ I. Kézsmárki *et al.*, Phys. Rev. Lett. **93**, 266401 (2004).
- ²² S. T. Bramwell and M. J. P. Gingras, Science **294**, 1495 (2001), and references therein.
- ²³ The adaptation of the polarization modulation technique for Fourier transform infrared spectrometers will be published elsewhere by T. Ogasawara *et al.*
- ²⁴ Y. Yasui *et al.*, J. Phys. Soc. Jpn. **70**, 284 (2001).
- ²⁵ In the simplest model E_0 can be expressed as bandwidth times $(\theta/\pi)^2$ (θ : tilting angle of the spins). According to the estimation $\theta \cong 5^{06,24}$, we have $E_0 \sim 0.002$ eV. However, the unusual temperature dependence of $\sigma_{xy}(\omega=0)$, observed all the way up to T_c , implies that E_0 is about one order of magnitude larger.

Figure Captions

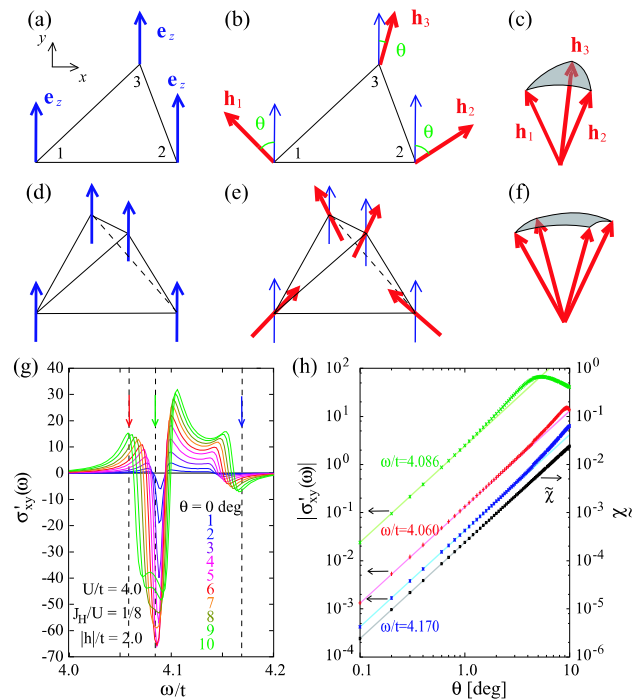


FIG. 1: (Color) (a) Collinear and (b) noncoplanar magnetic structures on a triangle cluster with the polar angle θ , and (c) the associated solid angle. (d) Collinear and (e) noncoplanar magnetic structures on a tetrahedron, and (f) the associated solid angle. (g) $\sigma'_{xy}(\omega)$ as a function of θ for the two-band Hubbard model on a triangle cluster. (h) Scaling plot of $|\sigma'_{xy}|$ vs θ at three energies denoted by the arrows in (g). Lines are fits to the θ^2 dependence.

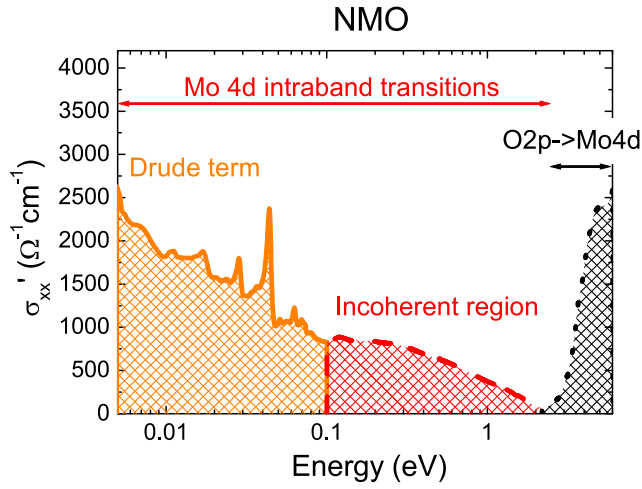


FIG. 2: (Color online) Real part of the diagonal conductivity $\sigma'_{xx}(\omega)$ in the ground state of NMO. The region of the Mo $4d$ intraband transitions and the O $2p \rightarrow$ Mo $4d$ charge-transfer excitations are indicated. The former is further divided into two parts: Drude term and mid-infrared incoherent excitations.

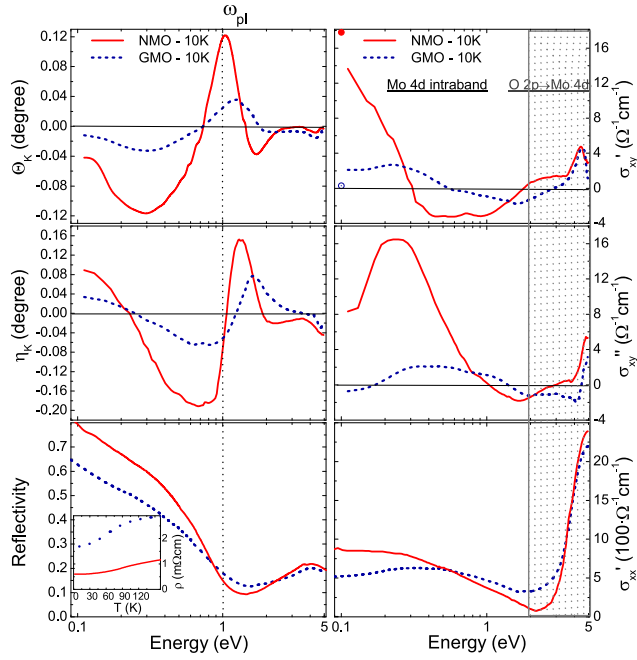


FIG. 3: (Color online) Left panels: Kerr rotation Θ_K , Kerr ellipticity η_K and reflectivity spectra of $\text{Nd}_2\text{Mo}_2\text{O}_7$ (NMO) and $(\text{Gd}_{0.95}\text{Ca}_{0.05})_2\text{Mo}_2\text{O}_7$ (GMO) measured at $T = 10$ K. The dotted line running through the plots indicates the plasma edge. The inset in the bottom panel shows the comparison of the dc resistivity for the two materials below $T = 160$ K. Right panels: Spectra of σ'_{xy} , σ''_{xy} , and σ'_{xx} at 10 K. In the top panel, the dc values σ_{Hall} are also indicated by dots. The high-energy region dominated by charge-transfer excitations is distinguished from the Mo $4d$ intraband transitions by a gray pattern.

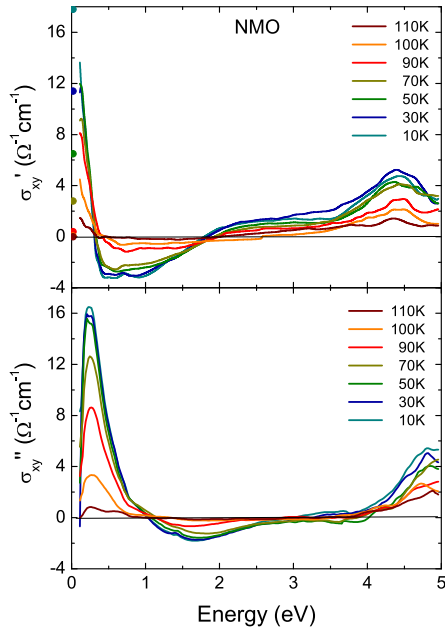


FIG. 4: (Color) Spectra of σ'_{xy} and σ''_{xy} of NMO at various temperatures. The corresponding dc values (σ_{Hall}) are also plotted with dots.

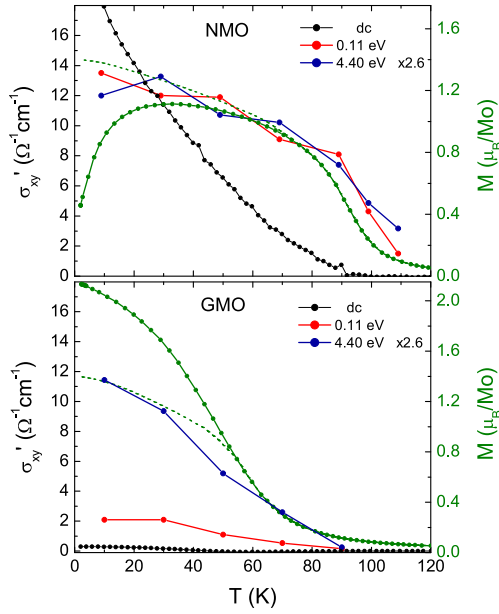


FIG. 5: (Color) The temperature dependences of $\sigma'_{xy}(\omega)$ and the magnetization both for NMO and GMO. $\sigma'_{xy}(\omega, T)$ is shown for three characteristic energies, $\omega = 0, 0.11$ and 4.4 eV by black, red and blue symbols, respectively. Note that the signal at 4.4 eV is multiplied with a factor of 2.6 . The overall magnetization is indicated by green symbols while the contribution of the Mo spins alone by a dashed line.